Chapter 5

Modification of CVM entropy functional for binary FCC phases using tetrahedron approximation

5.1 Introduction

In a binary FCC ordering prototype phase diagram, approximations using T and TO basic clusters yield different triple points involving $A1$, $L1_0$ and $L1_2$ phases for the same first neighbor pair interactions with the latter being relatively closer to the results of MCS (Finel and Ducastelle, 1986), (Kämmerer *et al.*, 1996). Finel used different combinations of approximations for the disordered phase and ordered phases, referred to as mixed CVM, namely, QT–TO (Finel, 1989) and 13-14 point clusters–TO ((13-14 pt)–TO) (Finel, 1994) for disordered and ordered phases respectively for exclusive first neighbour pair interactions and showed that they yield results in good agreement with the best known MCS results. Tepesch *et al.* (1998) showed that use of the CFs obtained by MCS in the CVM entropy functional corresponding to 13-14 point clusters (MCS-CVM-(13-14 pt)) for the disordered as well as ordered phases leads to good agreement with the best known results. The difference in the calculated phase diagrams in these approximations can be attributed primarily to the truncation of the entropy functional to different degrees of accuracy, as the enthalpy expression is identical in all these cases for exclusive first neighbour pair interactions.

Oates *et al.* (1999) have used tetrahedron as basic cluster in cluster site approximation (CSA–T) and modified the number of energetically non-interfering tetrahedron clusters per site in entropy functional for better agreement with the MCS

results. Although this methodology is able to correctly reproduce the topological features of the FCC prototype ordering phase diagrams, detailed agreement with the phase boundaries is less satisfactory. Jindal *et al.* (2014) have considered TO approximation of CVM and modified multiplicities of the basic clusters, namely, tetrahedron and octahedron clusters (MCVM–TO) only in the entropy functional such that the congruent points and the triple point in a binary FCC ordering prototype phase diagram are well reproduced. The computational burden involved in obtaining the equilibrium state of the system can be reduced further by considering a smaller basic cluster having less number of CFs for both the disordered as well as ordered phase, *i.e.*, first neighbour tetrahedron as basic cluster in CVM (CVM–T), as can be observed from the details of the CFs provided in Table 2.2 and the Appendix A.2 for T and TO approximations. However, the multiplicities of some of the subclusters also need to be modified in this approach. The reduction in the computational burden becomes significant especially for multicomponent systems, by as much as an order of magnitude. For FCC based prototypical ordering system, the accurate results are reported in literature only by considering $A1$, $L1_0$ and $L1_2$ phases. Accordingly, we have also considered only these three phases in this study, even though exclusive first neighbour pair interactions result in degenerate states.

The Au–Cu system exhibiting $A1$, $L1_0$ and $L1_2$ phases in the solid state is considered for testing the suitability of the above approximation. Golosov *et al.* (1973) demonstrated that three distinct maxima corresponding to the $A1$, $L1_0$ and $L1_2$ phases in the solid state arise in the phase diagram of a prototypical FCC ordering system such as Au–Cu computed using exclusive first neighbour pair interactions in CVM–T. However, they did not compute the triple points in the phase diagram. van Baal (1973) demonstrated the effect of multi-atom interactions using CVM–T in computing the FCC prototype ordering iso-Gibbs energy versus temperature diagrams. de Fontaine and Kikuchi (1978) have calculated the Au–Cu phase diagram considering multi-atom interactions using CVM–T, reproducing the main features of the phase diagram. Sundman *et al.* (1999) also assessed Au–Cu phase diagram, in which, the excess Gibbs energy was expressed using R-K polynomial for configuration - independent contributions, while the configuration-dependent contributions were modelled using CVM–T for the disordered and ordered solid phases. Oates *et al.* (1999) also have

calculated the phase diagram using CSA–T considering configurational energy as well as elastic energy arising due to lattice mismatch. The latter three efforts did not yield satisfactory agreement with the observed data.

The present contribution develops and demonstrates an empirical procedure for improving the accuracy of the CVM–T for binary FCC systems, using exclusive first neighbour pair interactions without increasing the computational burden, by suitably modifying the multiplicities (MCVM–T) of the basic cluster as well as some of the subclusters to reproduce the best-known critical temperatures as well as the triple point equilibrium corresponding to the results of MCS. Further, this MCVM–T is used to compute the optimized energy parameters and the Au–Cu phase diagram. The computed phase diagram is compared with the observed data and possible improvements in the methodology are identified.

5.2 Modification of CVM entropy functional

The configurational energy of mixing for the phases $A1$, $L1_0$ and $L1_2$ are expressed using the methodology discussed in the Section 2.2 and other contributions are not considered. In the present work, the consolute and congruent points, two phase and three phase equilibria are calculated using the algorithms discussed elsewhere (Gupta, 2008; Jindal, 2014).

The MCS data are available only for exclusive first neighbour pair interactions and are taken from various sources (given in Table 5.1) and used to optimize multiplicities in the entropy expressions. During the optimization process, the multiplicities of tetrahedron and triangle are altered together in a coupled manner such that the K-B coefficient of the triangle subcluster remains zero (as is the case when crystallographic multiplicities of FCC phase are used). This has been done to retain the simplicity of the CVM–T entropy functional. The multiplicity of the pair cluster is treated as another independent variable. Further, the modified multiplicities used in case of ordered structures are related to those of the disordered structure in a geometrically consistent manner. The multiplicities used in the internal energy expression are kept unchanged at the crystallographic values, since truncation effects are absent in the internal energy.

Table 5.1: Invariant reaction temperatures used in the optimization process and the temperatures obtained at different stages of the optimization process.

Invariant reaction	Invariant temperatures		
	best known value	computed using crystallographic m_i	computed using m_i^{Opt}
$A1 \leftrightarrow L1_0$	1.7386±0.0002 (Schweika, 1992)	1.8956	1.7358
$A1 \leftrightarrow L1_0$	1.86 (Binder, 1980)	1.94	1.86
$A1 \leftrightarrow L1_0 + L1_2$	0.98±0.02 (Kämmerer *et al.*, 1996)	1.62	0.98
$A1$ consolute temperature	9.81*(Schweika, 1992) 9.7956 (de Fontaine, 1994)	10.0254	10.9120

*Read from digitized Figure 1 of (Schweika, 1992)

A figure-of-merit function, χ^2, is defined as the sum of squares of the relative error between the observed and computed (using modified/variable multiplicities) values of the temperature of $L1_0$ and $L1_2$ congruent points and the triple point, as given below.

$$\chi^2 = \left(1 - \frac{T^{Calc}_{A1\leftrightarrow L1_0}}{T^{Best}_{A1\leftrightarrow L1_0}}\right)^2 + \left(1 - \frac{T^{Calc}_{A1\leftrightarrow L1_2}}{T^{Best}_{A1\leftrightarrow L1_2}}\right)^2 + \left(1 - \frac{T^{Calc}_{A1\leftrightarrow L1_0+L1_2}}{T^{Best}_{A1\leftrightarrow L1_0+L1_2}}\right)^2 \tag{5.1}$$

The equilibrium compositions of the phases are not considered for optimization, as MCS values are not available for all the invariant reactions. In addition, it is found that the changes in the crystallographic multiplicities required for reproducing the best-known values of (i) the consolute point temperature of the miscibility gap and (ii) the ordering system data are opposite in nature. Therefore, the consolute point temperature is not considered in the definition of the merit function. The merit function is minimized using Powell's algorithm (Acton, 1990; Press *et al.*, 2007) and refined manually to ensure accuracy up to 3rd decimal place for m_1 and m_2 ($m_3 = m_2/4$ to ensure that $\gamma_2 = 0$) and these are referred to as m_i^{Opt}.

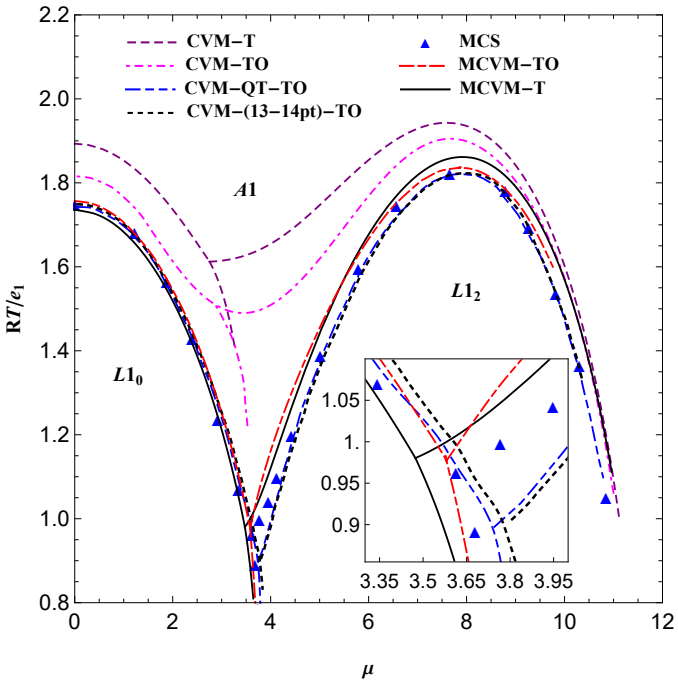

Figure 5.1: Potential versus temperature diagram for CVM with T, TO (Finel and Ducastelle, 1986), QT–TO (Finel, 1989), (13-14pt)–TO (Finel, 1994); MCS (Binder, 1980), (Kämmerer *et al.*, 1996), MCVM–TO (Jindal *et al.*, 2014) and MCVM–T [present investigation] approximations.

5.3 Results and discussion

5.3.1 MCVM–T approximation

The values of m_i^{Opt} corresponding to the tetrahedron, triangle and pair clusters are 1.32375, 5.295 and 6.833 respectively. The invariant temperatures for exclusive first neighbour pair interactions obtained by using these (MCVM–T) are given in Table 5.1. It can be observed that the invariant temperatures considered in the optimization are well reproduced with MCVM–T approximation. However, the consolute temperature shows an even larger departure from the MCS results than that obtained from CVM–T approximation.

The variation of a potential (μ), defined in Eq. (5.2) with respect to T for different approximations of CVM and MCS is given in Figure 5.1.

$$\mu = \frac{\mu_B - \mu_A}{2e_1} \tag{5.2}$$

where μ_A and μ_B are the chemical potentials of the components A and B respectively. It can be seen from Figure 5.1 that both the MCVM–TO and MCVM–T approximations yield results which are closely comparable to those of MCS and CVM - (13-14pt)–TO.

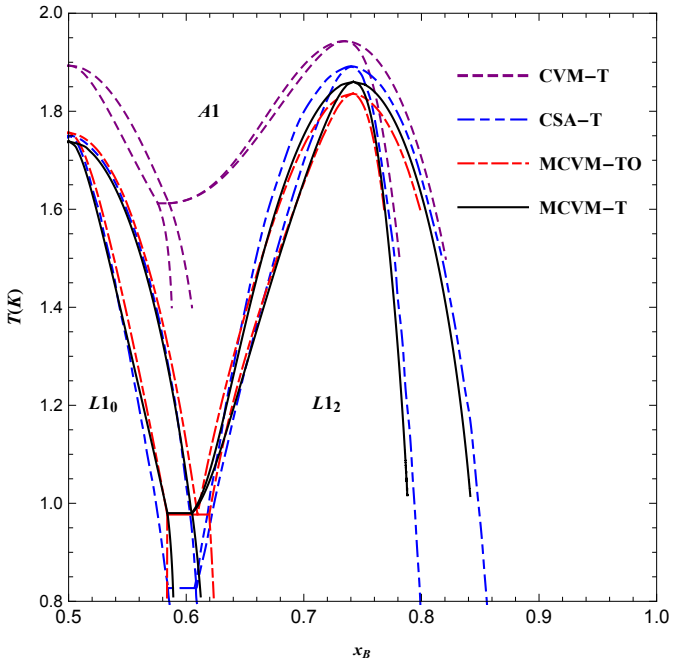

Figure 5.2: Comparison of phase diagram obtained using CVM–T, CSA–T (Oates *et al.*, 1999), MCVM–TO (Jindal *et al.*, 2014) and MCVM–T approximations.

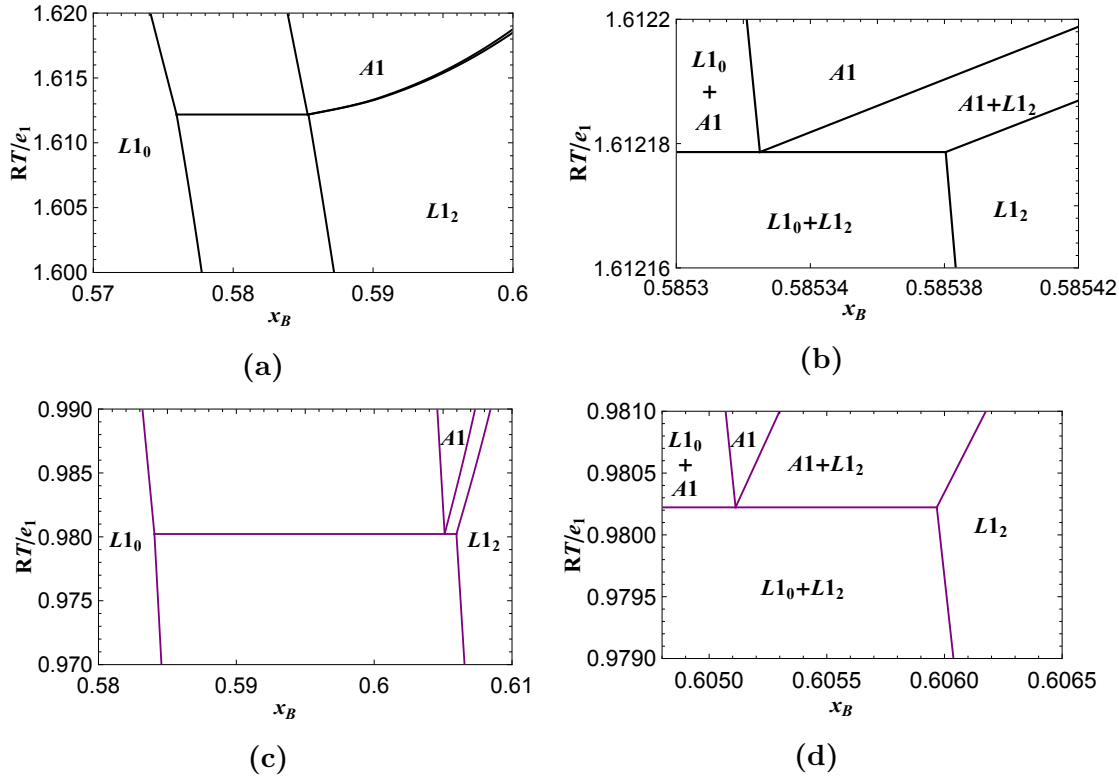

Figure 5.3: (a) The $A1 \leftrightarrow L1_0 + L1_2$ invariant reaction computed using CVM–T approximation. (b) Same as (a), but on a magnified scale. (c) The $A1 \leftrightarrow L1_0 + L1_2$ invariant reaction computed using MCVM–T approximation. (d) Same as (c), but on a magnified scale. Note the difference in the invariant temperatures from Table 5.1.

The prototype ordering phase diagrams computed using CVM–T, CSA–T, MCVM–TO and MCVM–T approximations are given in Figure 5.2. Details of the phase relations near the triple point for CVM–T and MCVM–T approximations are shown in Figure 5.3.

The variation of order parameter with temperature is calculated for $L1_0$ phase at x_B = 0.5, 0.55 and 0.60 & for $L1_2$ phases at x_B = 0.70, 0.75 and 0.80 using CVM–T as well as MCVM–T approximations and is shown in Figure 5.4. In these plots, the temperature corresponding to Helmholtz energies being equal for both ordered and disordered phases is represented by T^0. The upper instability temperature, T^+, corresponds to the temperature at which, the ordered phase becomes unstable and spontaneously transforms to its disordered counterpart while heating. Similarly, the lower instability temperature, T^-, corresponds to the temperature at which, the disordered phase spontaneously transforms to its ordered counterpart while cooling (Singh *et al.*, 2004; Soffa and Laughlin, 1989). The lower instability temperature is also referred to as spinodal ordering temperature (de Fontaine, 1994). The spinodal ordering boundaries are computed and depicted in Figure 5.5 for the cases of CVM–T and MCVM–T approximations. It can be observed from these figures that the order of transformation does not change in spite of the changes in the multiplicities in the MCVM–T approximation.

In addition to the phase diagrams, configurational energy of mixing (U^{mix}/e_1) is also calculated at $x_B = 0.5$ and 0.75 as a function of dimensionless temperature T/T_c (scaled with respect to the corresponding congruent temperature, T_c). The calculated thermodynamic data are compared with the MCS data (Jindal *et al.*, 2014) and are shown in Figure 5.6.

At $x_B = 0.5$, it can be observed that energy of mixing for the ordered phase is overestimated by MCVM–T compared to MCVM–TO and MCS. However, for the disordered phase, it is underestimated around the congruent temperature. In the case of $x_B = 0.75$, (U^{mix}/e_1) is overestimated by both MCVM–T and MCVM–TO for $L1_2$ phase and underestimated for $A1$ phase around the congruent point. However, the thermodynamic data computed using MCVM–T are in much better agreement with those obtained using MCS compared to CVM–T.

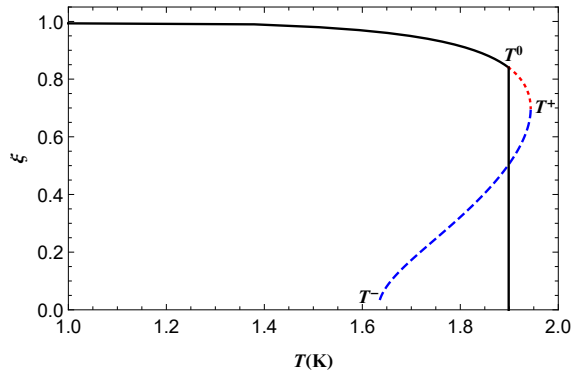

(a) $L1_0$, CVM–T, x_{B}=0.50

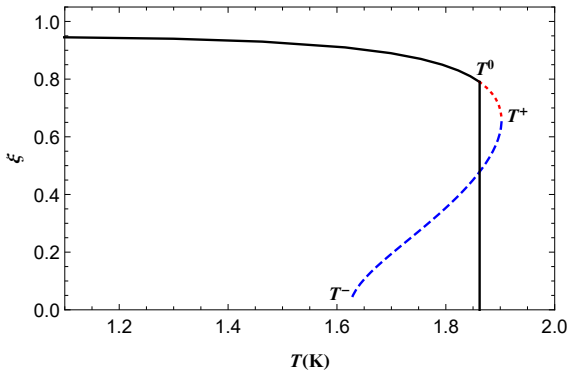

(b) $L1_0$, CVM–T, x_{B}=0.55

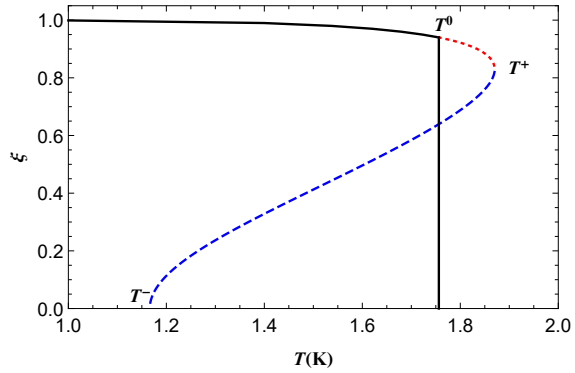

(c) $L1_0$, MCVM–T, x_{B}=0.50

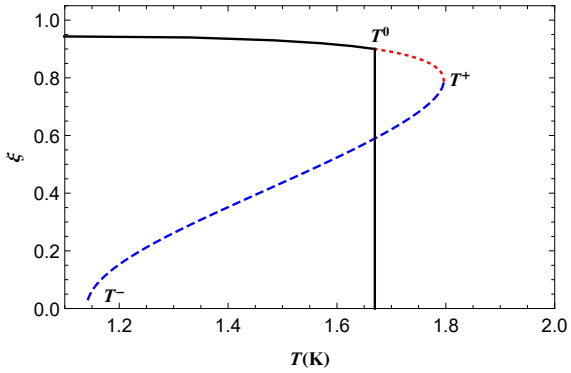

(d) $L1_0$, MCVM–T, x_{B}=0.55

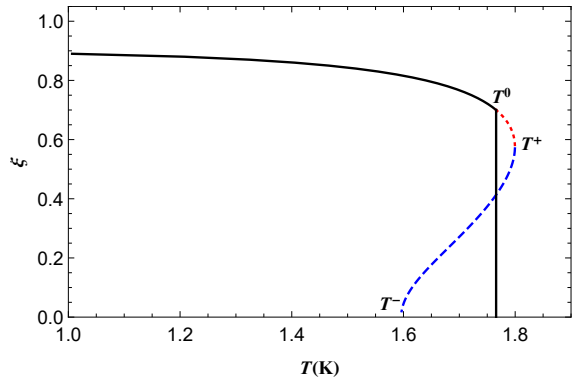

(e) $L1_0$, CVM–T, x_{B}=0.60

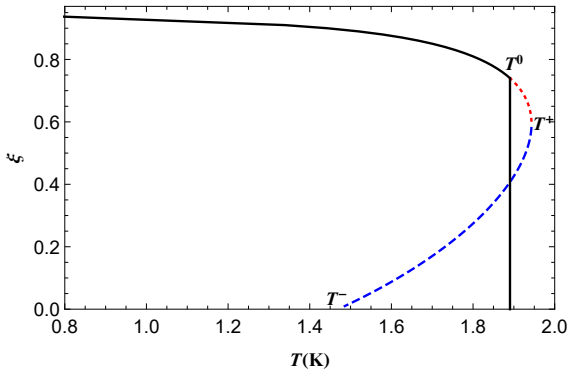

(f) $L1_2$, CVM–T, x_{B}=0.70

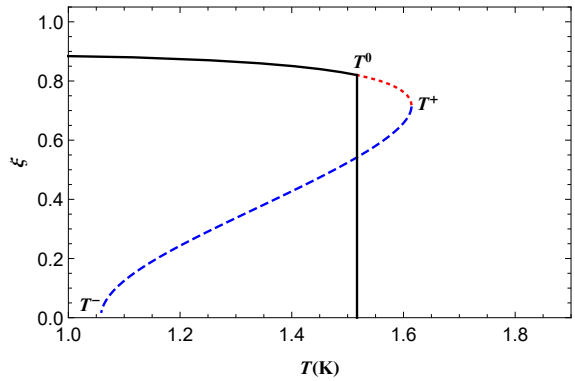

(g) $L1_0$, MCVM–T, x_{B}=0.60

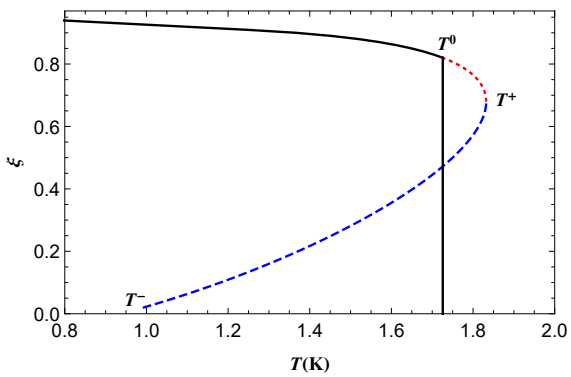

(h) $L1_2$, MCVM–T, x_{B}=0.70

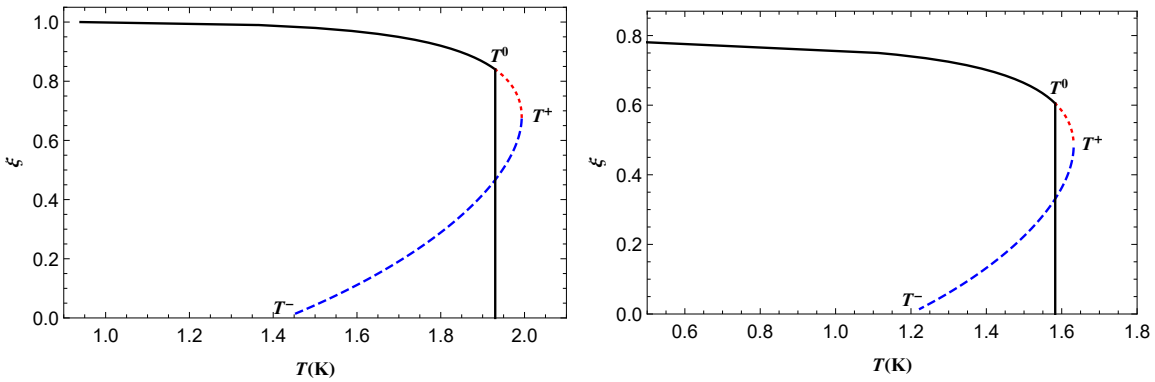

(i) $L1_2$, CVM–T, x_B=0.75 **(j)** $L1_2$, CVM–T, x_B=0.80

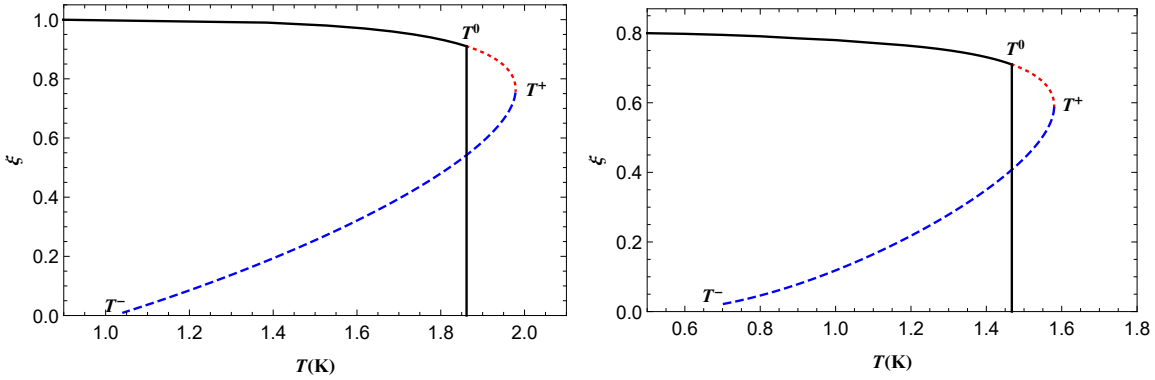

(k) $L1_2$, MCVM–T, x_B=0.75 **(l)** $L1_2$, MCVM–T, x_B=0.80

Figure 5.4: Variation of order parameter with temperature for $L1_0$ and $L1_2$ phases at various compositions.

In addition, (U^{mix}/e_1) is calculated as a function of composition at $RT/e_1 = 2$, while the configurational entropy of mixing (S^{mix}/R), is computed at $RT/e_1 = 1.9$ for a system with ordering tendency. A comparison of these results with those of MCS is given in Figure 5.7, which shows that both these quantities are improved due to modification of multiplicities. Even though the optimization is carried out considering only the invariant temperatures, agreement between the variation of thermodynamic properties with respect to temperature as well as composition is also improved (see Figure 5.6 and Figure 5.7).

For phase separating systems, the miscibility gap boundaries calculated using different approximations of CVM along with MCS data are shown in Figure 5.8. The phase boundaries for all the approximations given above are calculated for $e_{pair} = -R$. It can be observed that the miscibility gap boundary is rather poorly reproduced by MCVM–T. In particular, the consolute point temperature (cf. Table 5.1) as well as the curvature of the boundary involve significant error. However, one can treat the MCS data as experimental data and optimize the same to yield the CECs corresponding to

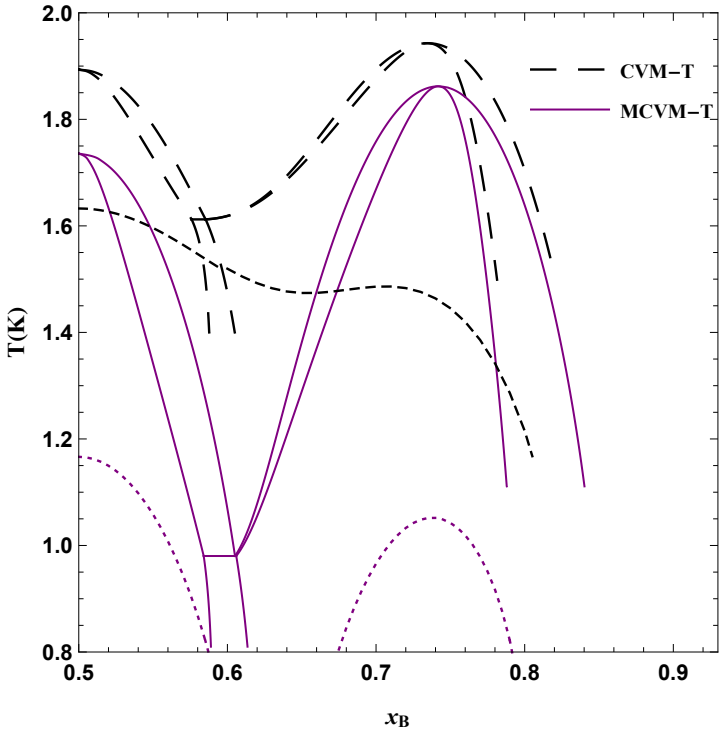

Figure 5.5: Prototype phase diagrams of an FCC ordering system computed using CVM–T and MCVM–T approximations. The spinodal ordering boundary corresponding to CVM–T is represented by (short) dashed line while that for MCVM–T is represented by dotted line.

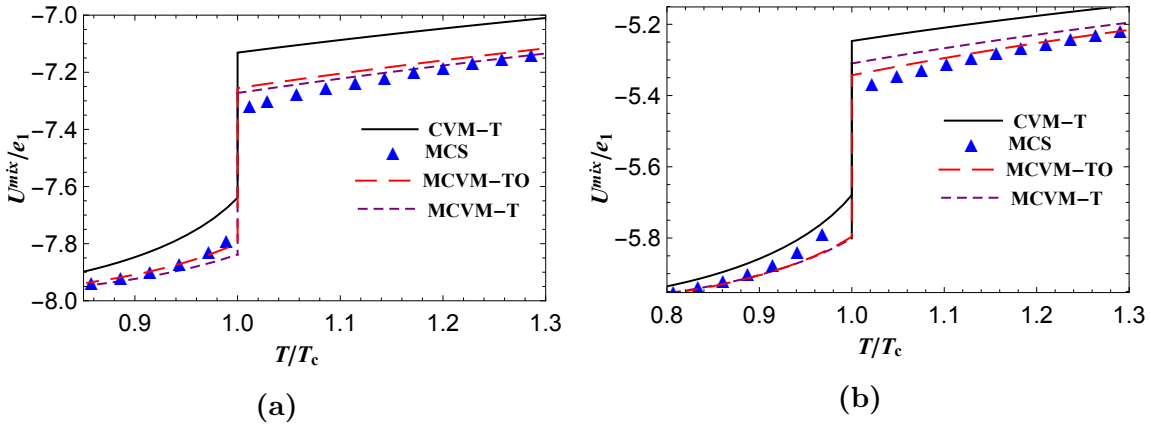

Figure 5.6: Variation of configurational internal energy of mixing (U^{mix}/e_1) as a function of reduced temperature (T/T_c) corresponding to CVM–T, MCS (Jindal *et al.*, 2014), MCVM–TO (Jindal *et al.*, 2014) and MCVM–T approximations at (a) $x_B = 0.5$ and (b) $x_B = 0.75$.

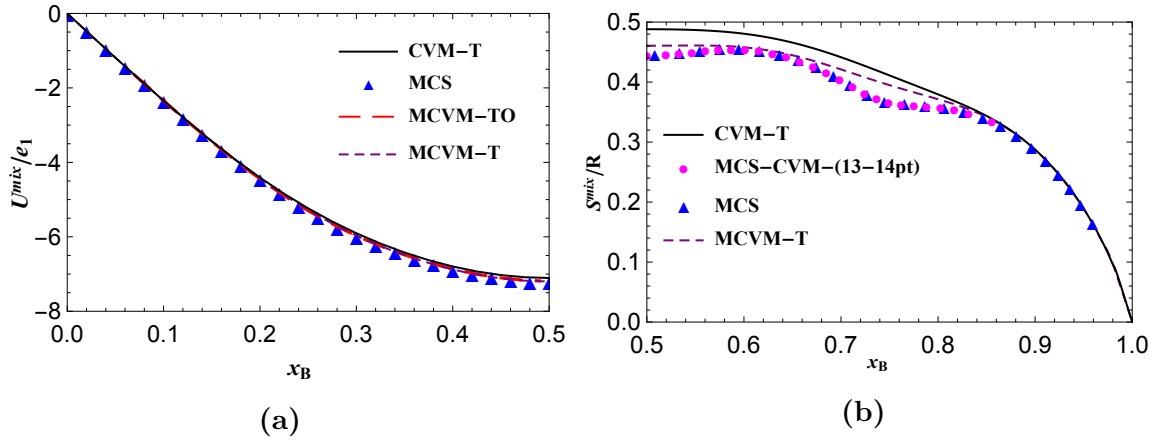

Figure 5.7: Variation of (a) U^{mix}/e_1 at $RT/e_1 = 2$ and (b) S^{mix}/R at $RT/e_1 = 1.9$ as a function of composition for a system having ordering tendency. The MCS data are taken from (Jindal *et al.*, 2014) and (Tepesch *et al.*, 1998), while the MCS-CVM–(13-14pt) data are taken from (Tepesch *et al.*, 1998).

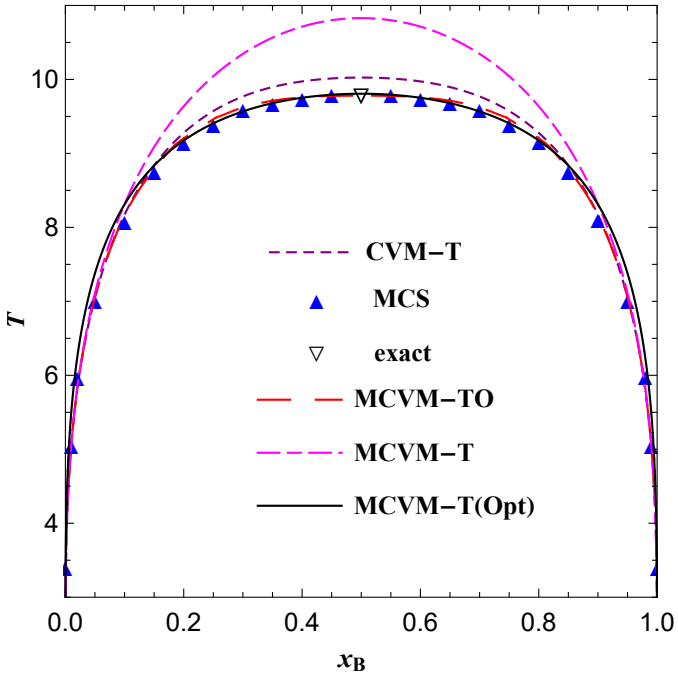

Figure 5.8: Comparison of miscibility gap boundary calculated using CVM–T, MCS (Schweika, 1992), exact (de Fontaine, 1994), MCVM–TO (Jindal *et al.*, 2014) and MCVM–T (present investigation) approximations.

best fit. Such a procedure leads to miscibility gap boundary shown in Figure 5.8 and labelled with MCVM–T(Opt). This boundary is calculated with the optimized energy parameters, namely, $(e^{Opt}_{pair}, e^{Opt}_{triangle}, e^{Opt}_{tetrahedron})/e_{pair} = (0.8464, 0, 0.3919)$, which is in much better agreement with the MCS results. We conclude that the topology of the experimental miscibility gap boundaries can be successfully reproduced by MCVM–T.

However, the optimized CECs correspond to a state of the system which is significantly different from the true thermodynamic state. As an example, the molar Gibbs energy of mixing calculated at $x_{\mathrm{B}} = 0.5$ and $T = T_{\mathrm{c}}^{Opt}$ using the modified multiplicities and optimized CECs is equal to -9.9074 J mol^{-1}, while the corresponding value at the same x_{B} and T using MCVM–TO and only $e_{pair} = -\mathrm{R}$ is equal to -10.6107 J mol^{-1}.

Thus, modification of multiplicities using a smaller cluster in CE–CVM is able to reproduce the best-known results of MCS or CE–CVM using larger clusters for ordering and phase separating tendencies of the FCC system.

5.3.2 Au–Cu phase diagram

The applicability of MCVM–T approximation to compute the Au–Cu phase diagram is tested by considering only configurational contributions to Gibbs energy (by neglecting any effects arising due to changes in the volume of the phases) and requiring that the three critical temperatures (namely, $A1 \leftrightarrow$ Au_3Cu ($L1_2$), $A1 \leftrightarrow$ AuCu ($L1_0$) and $A1 \leftrightarrow$ $AuCu_3$ ($L1_2$)) are reproduced, without attempting to optimize the entire phase diagram data. In this phase diagram, the long period superlattice (LPS) structures, namely, AuCu(II) and $AuCu_3$(II) phases are not considered since they cannot be modelled using T approximation of CVM. Such phases require approximations of CVM using larger clusters (Zhang and Sluiter, 2016) or models such as Axial-Next-Nearest-Neighbour-Ising (ANNNI) model (de Fontaine and Kulik, 1985). Owing to high structural similarity, the energy differences between AuCu(I) & AuCu(II) and $AuCu_3$(I) & $AuCu_3$(II) are quite small. Hence, in the present optimization the &phase equilibria with the disordered phases are approximated with AuCu(I) and $AuCu_3$(I) phases neglecting the LPS phases as done by researchers in all previous optimization efforts (Ferreira *et al.*, 1987; Kikuchi and de Fontaine, 1978; Oates *et al.*, 1999; Sundman *et al.*, 1999). The critical temperature corresponding to $A1 \leftrightarrow$ Au_3Cu ($L1_2$) has been chosen to be equal to the average of the two transus temperatures at $x_{\mathrm{Cu}} = 0.25$. This is done as $A1$ phase does not directly transform to Au_3Cu ($L1_2$) phase. A merit function, χ^2, similar to the one given in Eq. (5.1), is defined considering the three invariant temperatures.

$$\chi^2 = \left(1 - \frac{T^{Calc}_{A1\leftrightarrow \mathrm{Au_3Cu}}}{T^{Obs}_{A1\leftrightarrow \mathrm{Au_3Cu}}}\right)^2 + \left(1 - \frac{T^{Calc}_{A1\leftrightarrow \mathrm{AuCu}}}{T^{Obs}_{A1\leftrightarrow \mathrm{AuCu}}}\right)^2 + \left(1 - \frac{T^{Calc}_{A1\leftrightarrow \mathrm{AuCu_3}}}{T^{Obs}_{A1\leftrightarrow \mathrm{AuCu_3}}}\right)^2 \tag{5.3}$$

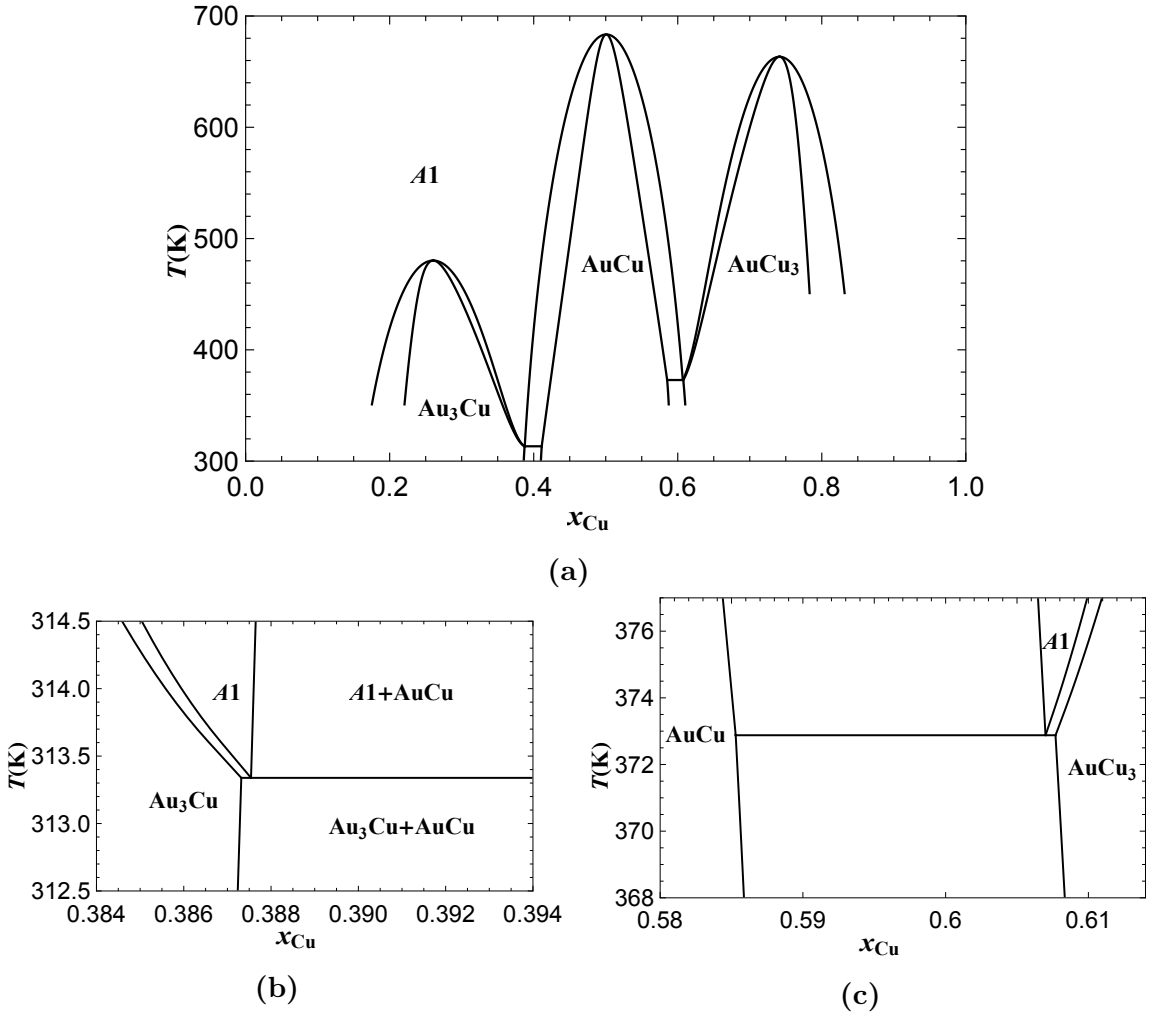

Figure 5.9: Au–Cu phase diagram calculated using MCVM–T approximation.

Using a standard nonlinear least squares optimization method called Levenberg - Marquardt method (Press *et al.*, 2007), the optimized CECs are calculated as (2920, 104, 191) J mol^{-1} respectively for pair, triangle and tetrahedron clusters. The computed phase diagram is given in Figure 5.9, while the calculated and observed invariant temperatures are given in Table 5.2.

It may be noted that the invariant reactions on either side of the equi-atomic composition are of eutectoid type in contrast to those in the experimental diagram. Further, the calculated eutectoid temperature for $x_{\mathrm{Cu}} < 0.5$ is lower than the observed peritectoid temperature by almost 200 K, while that for $x_{\mathrm{Cu}} > 0.5$ is lower by 185 K than its observed counterpart. The observed phase diagram reported by Okamoto *et al.* (1987), from which the transformation temperatures are considered in this optimization is shown in Figure 5.10 (a) while the comparison of the phase

Table 5.2: Observed and computed (using MCVM–T approximation) invariant temperatures in Au–Cu phase diagram. The presence of LPS structures is disregarded.

Reaction	Temperature (K)	
	Observed (Okamoto *et al.*, 1987)	Calculated
$A1 \leftrightarrow Au_3Cu$	480#	480
$A1 \leftrightarrow AuCu + Au_3Cu$	513*	313
$A1 \leftrightarrow AuCu$	683	683
$A1 \leftrightarrow AuCu + AuCu_3$	558	373
$A1 \leftrightarrow AuCu_3$	663	663

the average of the two transus temperatures as mentioned in the text
* corresponds to peritectoid reaction

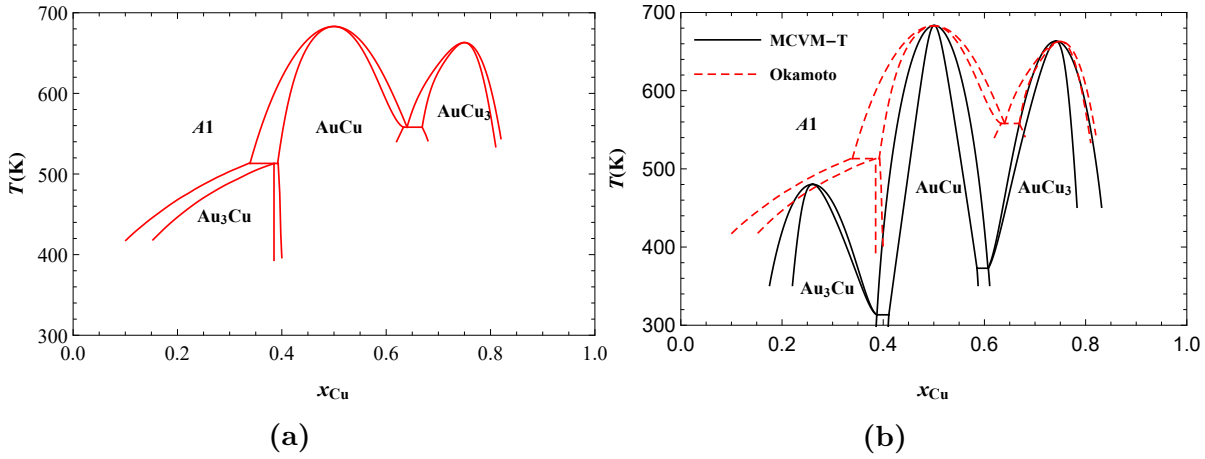

Figure 5.10: The Au–Cu phase diagram (a) reported by Okamoto *et al.* (1987) and (b) comparison with MCVM–T approximation.

diagram optimized for specific transformation temperatures with that of the actual one can be found in Figure 5.10 (b). Hence, it is clear that it is not possible to obtain the observed topology of the phase diagram using configurational contributions alone in the present approximation. Further, the widths of the single and two-phase fields in the computed phase diagram bear no resemblance to the observed ones.

Inclusion of non-configurational effects such as elastic contributions (Ferreira *et al.*, 1987), vibrational and electronic contributions (Asta *et al.*, 1993) leads to major changes in the topology of the phase diagram including the widths of single and two-phase fields, and are likely to yield better agreement with the observed phase diagram. Another significant effect is the likely dependence of CECs on the CFs due to truncation of CE as shown recently by Sanchez (2019). It is shown by Kikuchi (1998) that introduction of size effects leads to change in the transition temperature

as well the shift of the phase boundaries towards smaller atoms. The consequences of these effects need to be explored for application to real systems such as Au–Cu.

5.4 Conclusions

The crystallographic values of multiplicities in the entropy functional for CVM–T have been modified in order to represent the best-known results in FCC prototype ordering systems with exclusive first neighbour pair interactions, since such results are available only for this case. Such a modification reproduces the desired topology of the prototype FCC ordering phase diagram extremely well. In addition, the configurational energy and entropy of the ordering system approach the MCS results indicating improvement even in the thermodynamic representation of the system in comparison with CVM–T.

However, it was found that the multiplicities need to be altered in opposite directions for phase separating and ordering tendencies. Due to the opposing requirements of modification in the crystallographic values of the multiplicities, the present modification led to a significant departure of the computed consolute temperature and miscibility gap boundary from the best known results. To mimic optimization of an experimentally determined phase diagram, the best-known results of the miscibility gap boundary in a prototype phase separating system have been optimized to determine CECs. The boundary is now well reproduced albeit with slightly incorrect values of the CECs.

CE–CVM using a smaller cluster but with modified multiplicities is able to reproduce the best-known results of MCS or CE–CVM using larger clusters for ordering as well as phase separating tendencies of the FCC system. Although, there is a departure in the representation of the configurational state and thermodynamics of the system in the latter case, the same is within usual experimental error bounds.

This phenomenological approach improves the quality of results obtained from the lower approximation, without increasing the computational burden and not significantly sacrificing the SRO information. Overall, it must be recognised that this provides a much better model than the current CALPHAD methods. Clearly this approximation cannot be used where next nearest neighbour pairwise interactions are significant and become necessary to break the degeneracy between, say, $L1_2$ and

$D0_{22}$ phases. However, it is quite common to use different thermodynamic models for different phases in an alloy system as well as different models for a phase based on the same structure in different alloy systems.